



Multiple Outbursts of Asteroid (6478) Gault*

Quanzhi Ye (叶泉志)^{1,2}, Michael S. P. Kelley³, Dennis Bodewits⁴, Bryce Bolin^{5,6,11}, Lynne Jones⁵, Zhong-Yi Lin (林忠義)⁷, Eric C. Bellm⁵, Richard Dekany⁸, Dmitry A. Dhev¹, Steven Groom², George Helou², Shrinivas R. Kulkarni¹, Thomas Kupfer⁹, Frank J. Masci², Thomas A. Prince¹, and Maayane T. Soumagnac¹⁰

¹Division of Physics, Mathematics and Astronomy, California Institute of Technology, Pasadena, CA 91125, USA; qye@caltech.edu

²Infrared Processing and Analysis Center, California Institute of Technology, Pasadena, CA 91125, USA

³Department of Astronomy, University of Maryland, College Park, MD 20742, USA

⁴Department of Physics, Auburn University, Auburn, AL 36849, USA

⁵DIRAC Institute, Department of Astronomy, University of Washington, 3910 15th Avenue NE, Seattle, WA 98195, USA

⁶B612 Asteroid Institute, 20 Sunnyside Avenue, Suite 427, Mill Valley, CA 94941, USA

⁷Institute of Astronomy, National Central University, 32001, Taiwan

⁸Caltech Optical Observatories, California Institute of Technology, Pasadena, CA 91125, USA

⁹Kavli Institute for Theoretical Physics, University of California, Santa Barbara, CA 93106, USA

¹⁰Department of Particle Physics and Astrophysics, Weizmann Institute of Science 234 Herzl Street, Rehovot, 76100, Israel

Received 2019 February 20; revised 2019 March 6; accepted 2019 March 8; published 2019 March 29

Abstract

Main-belt asteroid (6478) Gault unexpectedly sprouted two tails in late 2018 and early 2019, identifying it as a new active asteroid. Here we present observations obtained by the 1.2 m Zwicky Transient Facility survey telescope that provide detailed time-series coverage of the onset and evolution of Gault's activity. Gault exhibited two brightening events, with the first one starting on 2018 October 18 \pm 5 days and a second one starting on 2018 December 24 \pm 1 days. The amounts of mass released are 2×10^7 kg and 1×10^6 kg, respectively. Based on photometric measurements, each event persisted for about a month. Gault's color has not changed appreciably over time, with a pre-outburst color of $g_{PS1} - r_{PS1} = 0.50 \pm 0.04$ and $g_{PS1} - r_{PS1} = 0.46 \pm 0.04$ during the two outbursts. Simulations of dust dynamics shows that the ejecta consists of dust grains of up to 10 μ m in size that are ejected at low velocities below 1 m s⁻¹ regardless of particle sizes. This is consistent with non-sublimation-driven ejection events. The size distribution of the dust exhibits a broken power law, with particles at 10–20 μ m following a power law of -2.5 to -3.0 , while larger particles follow a steeper slope of -4.0 . The derived properties can be explained by either rotational excitation of the nucleus or a merger of a near-contact binary, with the latter scenario to be statistically more likely.

Key words: comets: individual ((6478) Gault) – minor planets, asteroids: individual ((6478) Gault)

Supporting material: animation

1. Introduction

The active asteroids make up a small-body population in our solar system that is dynamically asteroids, but can transiently or periodically display comae and tails. While the activity of comets is driven by sublimation, asteroid activity may be driven by a diverse set of mechanisms, including sublimation, rotational instability, impacts, and thermal fracturing (Jewitt et al. 2015). The occurrence rate of active asteroids is about 1–10 per 100,000 (see Chandler et al. 2018), implying <100 active asteroids among the known $\sim 800,000$ asteroids.

(6478) Gault is a kilometer-sized asteroid in the Phocaea family (Nesvorný 2015) with no previous record of activity. With a Tisserand parameter with respect to Jupiter, $T_J = 3.46$,¹² Gault is dynamically a main-belt asteroid. Its activity was first detected by the Asteroid Terrestrial-impact Last Alert System (ATLAS) on 2018 December 8 (Smith et al. 2019),

with confirmations by other observers (e.g., Hale et al. 2019; Jehin 2019; Ye et al. 2019).

We identified serendipitous observations of Gault in the Zwicky Transient Facility (ZTF) survey data, dating back to 2017 November 14. These observations provide baseline (inactive) photometry as well as extended coverage of the activation of Gault. In this Letter, we analyze the time-series data provided by ZTF to characterize the activity of Gault, and to understand the mechanism that drove its activity.

2. Observations

ZTF is a synoptic survey combining the 1.2 m Oschin Schmidt telescope with a new 47 deg² camera at Palomar Observatory. Using 30 s exposures, ZTF can observe an area of 3760 deg² in an hour, to a typical 5σ detection limit of $r_{PS1} = 20.7$. Most survey observations are taken in the ZTF g and r filters. The telescope and its survey strategy are described in Bellm et al. (2019) and Graham et al. (2019).

We use ZChecker,¹³ a software suite originally developed to analyze comet images in ZTF data, to extract and process the ZTF images of Gault (Kelley et al. 2019). ZChecker uses the ephemeris provided by JPL HORIZONS (Giorgini 2015) and the survey metadata (Masci et al. 2019) to identify observations of known small bodies in the ZTF archive.

* Data and codes that generate the figures of this work are available on Zenodo (doi:10.5281/zenodo.2590809) and at https://github.com/Yeqzids/activation_of_6478_gault.

¹¹ B612 Asteroid Institute and DIRAC Institute Postdoctoral Fellow.

¹² From JPL solution #21, retrieved on 2019 February 10.



¹³ <https://github.com/mkelley/zchecker/>

The software combines frames from each night into nightly stacks, and applies temporal filtering to the images to highlight morphological changes over time. Based on ZChecker identified observations, we derived photometry based on point-source-function (PSF) fitting from the ZTF data reduction pipeline (Masci et al. 2019), and extracted the source nearest the ephemeris position of Gault. Photometric zero-points for the absolute calibration are calculated by the ZTF Science Data System by comparing field stars with the PANSTARRS Data Release 1 catalog (see Magnier et al. 2013; Masci et al. 2019, Section 3.5).

ZTF has observed Gault more than 300 times since its commissioning in late 2017, with most observations occurring after 2018 October. A time-series animation of ZTF imaging of Gault is shown in Figure 1. The images shown are cut-out frames of $5' \times 5'$. Most stars are masked before the frames are median combined into nightly stacks. The total integration time each night varies from 30 s to 27 minutes.

3. Results

A summary of the ZTF photometry of Gault is shown in Figure 2. We first construct our own *HG* photometry model for Gault, as absolute magnitudes based on the Minor Planet Center (MPC) database contain biases of up to 0.3–0.5 mag (Jurić et al. 2002; Pravec et al. 2012). By using the observations acquired in 2017 (pre-outburst), we derive $H_g = 14.81 \pm 0.04$ and $H_r = 14.31 \pm 0.01$, assuming $G = 0.15$. This yields $g_{\text{PS1}} - r_{\text{PS1}} = 0.50 \pm 0.04$. The color is both broadly consistent with C-type asteroids ($g_{\text{PS1}} - r_{\text{PS1}} \approx 0.5$) and, to a lesser degree, with S-type asteroids and comets ($g_{\text{PS1}} - r_{\text{PS1}} \gtrsim 0.6$).

The light curve shows that Gault was already ~ 2 mag above baseline when ZTF observed it on UT 2018 October 31.50, the first ZTF observation in 2018. The asteroid was first point-source-like in appearance and its size was equivalent to the seeing (with FWHM of $\sim 2''$). The brightness peaked around 2018 November 7 with a final brightness increase of $\Delta\text{mag} = 2.4$. A tail first appeared in ZTF images from UT 2018 November 16. The light curve suggests that the brightening subsided around 2018 mid December.

The photometry shows that a second outburst started between UT 2018 December 24.51–28.46 and peaked near 2019 January 4, with $\Delta\text{mag} = 0.6$ compared to the subsided brightness in 2018 mid December (accounting for the change of geometry). The brightening lasted about 2 weeks. A new tail was first observed in ZTF images on 2019 January 28. This second tail was observed as early as 2019 January 20 by other observers (Jehin 2019; Lee 2019).

During both active phases, Gault had $g_{\text{PS1}} - r_{\text{PS1}} = 0.46 \pm 0.04$, in 1σ agreement with the color of the nucleus ZTF measured in 2017. The asteroid and its near-nucleus ejecta is thus slightly redder than the Sun ($g_{\text{PS1}} - r_{\text{PS1}} = 0.39$; see Willmer 2018). This suggests that the dust ejecta does not contain a preponderance of Rayleigh scatterers (i.e., sub- μm -sized dust) or water ice.

4. Analysis

4.1. Onset of Activity

The behavior of brightness over time can be used to determine the onset of activity and to characterize the ejecta. In

Figure 3 we note that the brightening phase appears to follow a square law:

$$I = z(t - t_0)^2, \quad (1)$$

where I is the excess flux, $t - t_0$ is the elapsed time since the start of activity, and z is a constant related to the acceleration of the dust grains. The underlying assumption is that (1) the ejecta is dominated by dust grains that do not fragment; (2) the brightness is proportional to the total surface area of the ejecta; and (3) either the full volume is optically thick until the peak brightness, or the dust is being continually produced for several days. An alternative scenario is that the fragmenting ejecta leads to an exponentially increasing brightness, as seen in cometary outbursts (e.g., Hsieh et al. 2010). The latter scenario cannot describe the light curve of Gault.

Based on Figure 3, the parameters most compatible with the observations are $t_0 = 2018 \text{ October } 18 \pm 5$, $z = 0.40 \pm 0.05 \text{ day}^{-2}$ for the first outburst, and $t_0 = 2018 \text{ December } 24 \pm 1$, $z = 0.10 \pm 0.02 \text{ day}^{-2}$ for the second outburst. The spread in z is likely an artifact due to the limited number of observations, especially for the second event.

4.2. Dust Properties

4.2.1. General Properties

To constrain the size of the dust grains in the ejecta and to provide an independent constraint on the onset of activity, we performed a syndyne-synchrone analysis (see Finson & Probst 1968) of the ZTF images. Syndynes are a set of lines representing the positions of particles of the same sizes, whereas synchrones are a set of lines representing the positions of particles released at the same time. Syndynes are usually expressed using β , the ratio of the solar radiation and gravitation forces and a proxy for particle size: $\beta = 5.74 \times 10^{-4}/(\rho r)$, where ρ is particle density and r is particle radius, both in MKS units.

We use images taken on 2018 December 29 and 2019 February 8 for our analysis. These images are selected due to their relatively high signal-to-noise ratios (S/Ns). Analysis with a finer time step did not provide extra information, because the event evolves over a timescale of weeks.

As shown in Figure 4, the primary tail most closely resembles the synchrone curves that reproduce materials released between 2018 late October and 2018 mid November, in agreement with the results above. The new, secondary tail is consistent with an onset around 2019 January 1, also consistent with the second onset date derived above (± 1 week from 2019 January 4).

The range of β values (i.e., grain sizes) can be estimated by matching the overlapping sections of the tail and the syndynes. We establish that the smallest grains released in both events have $\beta \approx 0.03$ (or approximately $15 \mu\text{m}$ in diameter) and the largest grains have at least $\beta = 0.001$ (or 0.4 mm in diameter).

The syndyne-synchrone analysis assumes zero terminal ejection speeds of dust grains, and therefore cannot be used to derive ejection speeds of the dust. However, the absence of Sun-ward ejecta can be used to constrain the ejection speed (e.g., Hui et al. 2017):

$$v_{\text{ej}} \leq \frac{(2\beta GM_{\odot} \Delta t)^{1/2}}{r_{\text{h}}}, \quad (2)$$

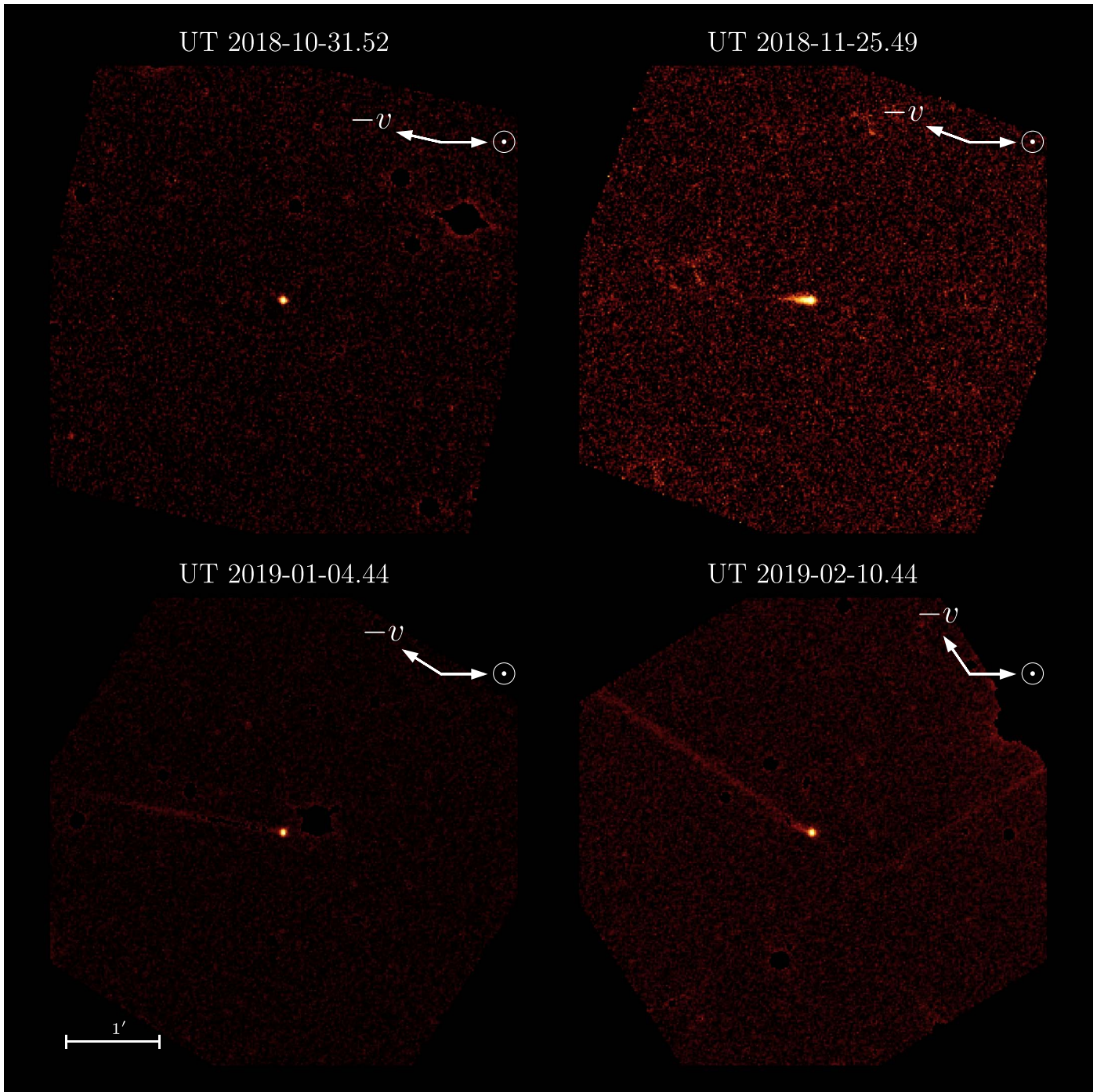


Figure 1. ZTF observations of the evolution of Gault’s activity from UT 2018 October 31 to 2019 February 10. Most background sources are masked, leaving a few artifacts. Frames are projected into a reference frame with the projected vector to the Sun in the $+x$ direction. The $-v$ vector points to the negative of the motion vector. The animation of the ZTF observations runs from 2018 October 31.52 to 2019 January 31.29 UT. Notebook is available here https://github.com/Yeqzids/activation_of_6478_gault/blob/master/img.ipynb.

(An animation of this figure is available.)

where $G = 6.67 \times 10^{-11} \text{ N kg}^2 \text{ m}^{-2}$ is the gravitational constant, $M_{\odot} = 2 \times 10^{30} \text{ kg}$ is the mass of the Sun, Δ and r_h are the geocentric and heliocentric distance, and $l \approx 1''$ is the apparent Sun-ward turnaround distance measured from the nucleus, as constrained by the PSF of our ZTF images. By substituting the variables with corresponding numbers and taking $\beta \leq 0.03$ (from the syndyne-synchrone analysis above),

$\Delta = 1.51 \text{ au}$ and $r_h = 2.41 \text{ au}$ for UT 2019 February 8.3, we obtain an upper limit of $v_{ej} \leq 8 \text{ m s}^{-1}$.

4.2.2. Dust Tail Model

The tail morphology can be used to further constrain the properties of the ejecta, and we employ the dust dynamics code

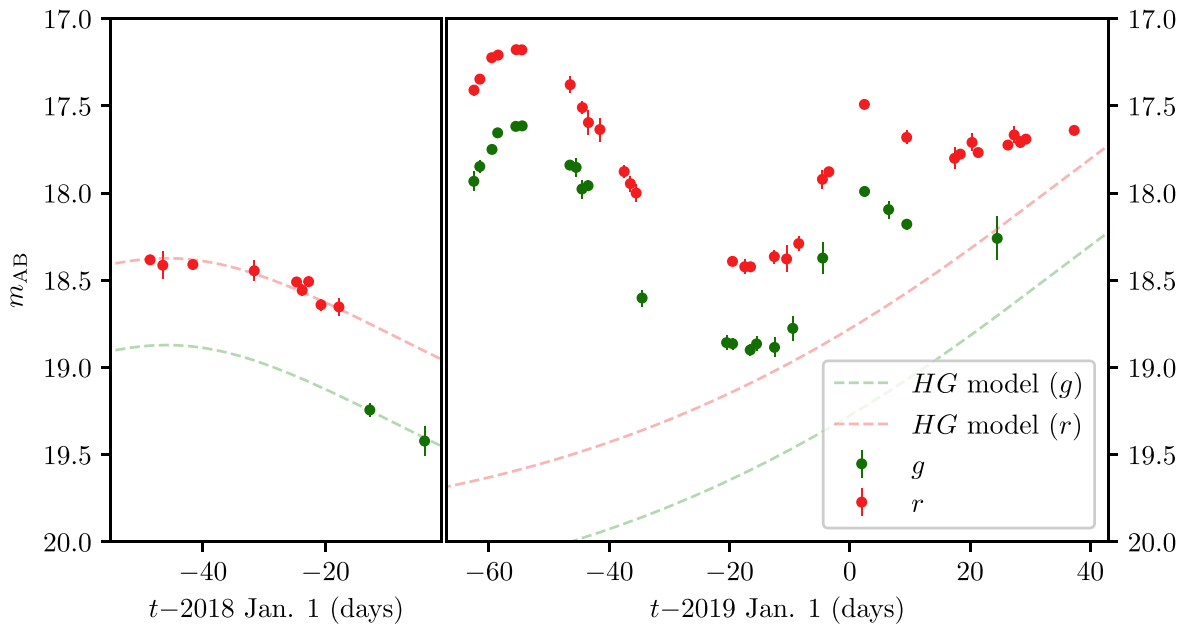


Figure 2. Long-term light curve of Gault in late 2017 (left panel) and late 2018 to early 2019 (right panel) constructed from nightly binned ZTF photometry. Also shown is the predicted baseline (i.e., inactive) brightness from our *HG* model. Notebook is available here https://github.com/Yeqzids/activation_of_6478_gault/blob/master/lightcurve.ipynb.

originally developed by Ye et al. (2016). We focus on the stacked image of 2019 February 8, as it offers the highest S/N in our data set, with both tails clearly visible. Although the model contains a number of poorly constrained parameters and often cannot provide unique solutions, for this particular case, the light-curve and syndyne-synchrone analysis above has provided a set of useful boundary conditions, which helps the identification of improbable solutions.

The model assumes isotropic ejection, with the terminal ejection speed defined as:

$$v_{ej} = V_0 \beta^p, \quad (3)$$

where V_0 is the mean terminal ejection speed of a $\beta = 1$ dust grain, and p is a constant. We will test V_0 of 1 and 8 m s^{-1} for $p = 0$, and $V_0 = 50 \text{ m s}^{-1}$ for $p = 0.5$. These values are chosen because (1) the range of V_0 is determined by the largest V_0 capable to launch particles from $30 \mu\text{m}$ to 1 mm into terminal speed, while not exceeding the 8 m s^{-1} limit derived above; and (2) it has been found that non-sublimation-driven active asteroids follow $p = 0$, while sublimation-driven active asteroids follow $p = 0.5$ (Moreno et al. 2012; Jewitt et al. 2015). We assume the dust size follows a simple power law, with a differential size index of q . The range of q to be tested is from -4.0 to -2.5 , a range identified by previous observations of comets and active asteroids (see Fulle 2004; Jewitt et al. 2015; Rotundi et al. 2015), with an interval of 0.5. The β of the test particles ranges from 0.0003 to 0.03 as indicated by Figure 4. Particles are released during 2018 November 7 ± 5 and 2019 January 4 ± 5 , the FWHM estimated from Figure 3. We assume the ratio between the dust productions of the two events is 16:1, in concordance with the amounts of mass losses derived later in Section 4.3.

Model images, shown in the upper panel of Figure 5, clearly show that only $V_0 = 1 \text{ m s}^{-1}$ and $p = 0$ agrees with the observation. This indicates that the dust grains are released just

beyond the gravitational escape speed of Gault. A constant ejection speed through the particle size range is in line with the behavior of other active asteroids with non-sublimation-driven ejection (Jewitt et al. 2015).

Since the tail is straight and narrow, we collapse the observational and model images into one-dimensional profiles along the tail axis for simple comparison. Note that the tail axis is 31° off from the Sun-comet axis in the counterclockwise direction, due to the coupling of gravitational attraction and radiation pressure on the dust grains. To minimize sky noise, the observational profile is derived from summing a $20''$ -wide strip along the tail axis, with the width of $20''$ corresponding to the width of the tail.

The profiles, shown in the lower panel of Figure 5, reveal a turnover point at $\sim 140''$ behind the nucleus, corresponding to particles with $\beta = 0.01$ according to the syndyne analysis in Figure 4. Particles with $\beta < 0.01$ follow $q = -4.0$ while those with $\beta > 0.01$ follow $q = -2.5$ to -3.0 . A quick check shows that the turnover is also seen in the data taken on 2019 January 28. A change in the power law of the dust size distribution is interesting but not unusual: similar behaviors have been observed in meteor observations (Ye et al. 2014) and in situ measurements (Gombosi 1986; Price et al. 2010), and probably reflect either inherent properties of individual comets or spaceweathering processes on different sizes of dust. Note that these materials are ejected during the first event; ejecta from the second event are within $40''$ from the nucleus and do not have as much statistics. We crudely estimate $q = -3.5$ to -4.0 for the ejecta from the second event.

4.3. Mass Loss

The total mass loss can be calculated by:

$$M_d = \frac{4}{3} \rho_d \bar{a} C_e, \quad (4)$$

where $\rho_d = 2900 \text{ kg m}^{-3}$ is the bulk density of dust grains (Carry 2012), \bar{a} is the characteristic grain size for the derived

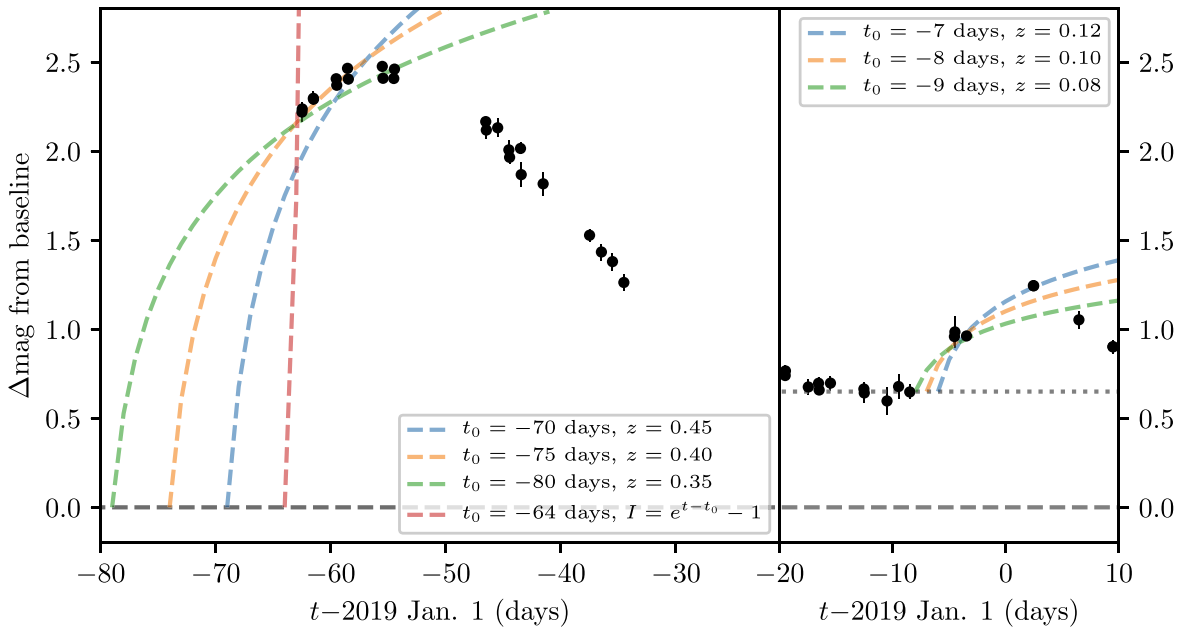


Figure 3. Brightness excess of Gault from the prediction by the *HG* model, with square-law and exponential functions matched to the data points. The left panel shows the first activation, the right panel the onset of the second. The dashed line is the baseline and the dotted line is the asymptote in 2018 mid December. Notebook is available here https://github.com/Yeqzids/activation_of_6478_gault/blob/master/lightcurve.ipynb.

size distribution, which we take $\beta = 0.01 \Leftrightarrow 20 \mu\text{m}$, following the results from Section 4.2, and C_e is the effective scattering cross-section of the ejecta:

$$C_e = \frac{\pi r_h^2 \Delta^2}{p_V \Phi(\alpha) a_\oplus^2} (10^{0.4 \Delta m_r} - 1) 10^{0.4(m_\odot, r - m_r)}, \quad (5)$$

where Δm_r is the brightness excess in r , $a_\oplus = 1.5 \times 10^{11}$ m is the mean heliocentric distance of the Earth, $\Phi(\alpha) = 0.035\alpha$ is the simple phase function of the target with a phase angle of α (see Li et al. 2015), $m_{\odot, r} = -26.9$ is the apparent r magnitude of the Sun (Willmer 2018), m_r is the nuclear brightness of the asteroid, and definitions of all other variables follow the definition in Equation (2). By substituting corresponding numbers from the two brightness peaks identified in Section 2, taking $\alpha = 21^\circ$ over the observed period and assuming $p_V = 0.04$ for the dust (Fulle et al. 2010), we obtain $M_d = 2 \times 10^7$ kg for the first event, and $M_d = 1 \times 10^6$ kg for the second event.

5. Activity Mechanism

Asteroid activity can be driven by a variety of mechanisms, including sublimation, impact, electrostatics, rotational excitation, thermal stress, or interactions of near-contact binaries (Taylor & Margot 2014; Jewitt et al. 2015). Our observations rule out sublimation (see Section 4.2.2) or electrostatics (which operates on micrometer-sized dust). Gault’s orbit keeps it relatively far from the Sun, ruling out thermal stress. Three possibilities seem to remain: impacts, rotational excitation, and binary interactions.

Gault is likely between 2 and 10 km in diameter, as estimated from our *HG* model. This number is calculated using the canonical relation $D = 1329 p_V^{-1/2} 10^{-H/5}$, where $p_V = 0.03\text{--}0.6$ is the geometric albedo of the Phocaea asteroids (Novaković et al. 2017). The albedo of Gault is not known. The broadband color derived from pre-outburst ZTF data is slightly

more compatible with low-albedo, C-type asteroids than other types of asteroids (see Section 3), but this needs spectroscopy to confirm.

Statistical models predict that for asteroids in this size range (i.e., asteroid with diameters of >2 km), impact-driven activity disruption occurs more frequently than rotation-driven activity (Marzari et al. 2011). However, the repeated activation of Gault would require multiple impacts, which we consider unlikely.¹⁴ If the two events were indeed driven by impacts, a pair of 10–20 m projectiles was needed to reproduce the observed brightness increase and the cross sections of the ejecta (Jewitt et al. 2015, Figure 16). A rotation-driven event, though consistent with the observation, occur at a rate of $10^{-6}\text{--}10^{-4} \text{ yr}^{-1}$ for the entire population of >2 km main-belt asteroids, which is low.

The most likely scenario, a merging near-contact binary, was suggested to drive the activity of 311P/PANSTARRS (Hainaut et al. 2014). A binary system can merge into a contact binary through the loss of angular momentum (known as the binary Yarkovsky–O’Keefe–Radzievskii–Paddack effect, or BYORP, see Ćuk & Burns 2005), but the merging process can cause fragmentation and dust emissions. Multiple ejection episodes may therefore be caused by different stages in the merging process. The timescale of the BYORP process is $\sim 10^5$ yr for near-Earth asteroids (Ćuk 2007), or $\sim 10^6$ yr for main-belt asteroids after accounting for lower solar radiation at larger distances to the Sun. Assuming 15% binaries among main-belt asteroids (see the discussion in Margot et al. 2015, Section 2.2), the rate of binary merges is (number of kilometer-sized main-belt asteroids) \times (fraction of binaries) \div (timescale of BYORP process) $= 10^6 \times 15\% \div 10^6 \text{ yr} = 0.1 \text{ yr}^{-1}$, which, for kilometer-sized asteroids, is much higher than the rates of impact- and rotation-driven activities for kilometer-sized asteroids.

¹⁴ An impact-driven activity would have been an excellent tribute to Dr. Donald Gault, whom the asteroid was named after; he was a pioneer in the field of impact cratering processes (Schultz 1999).

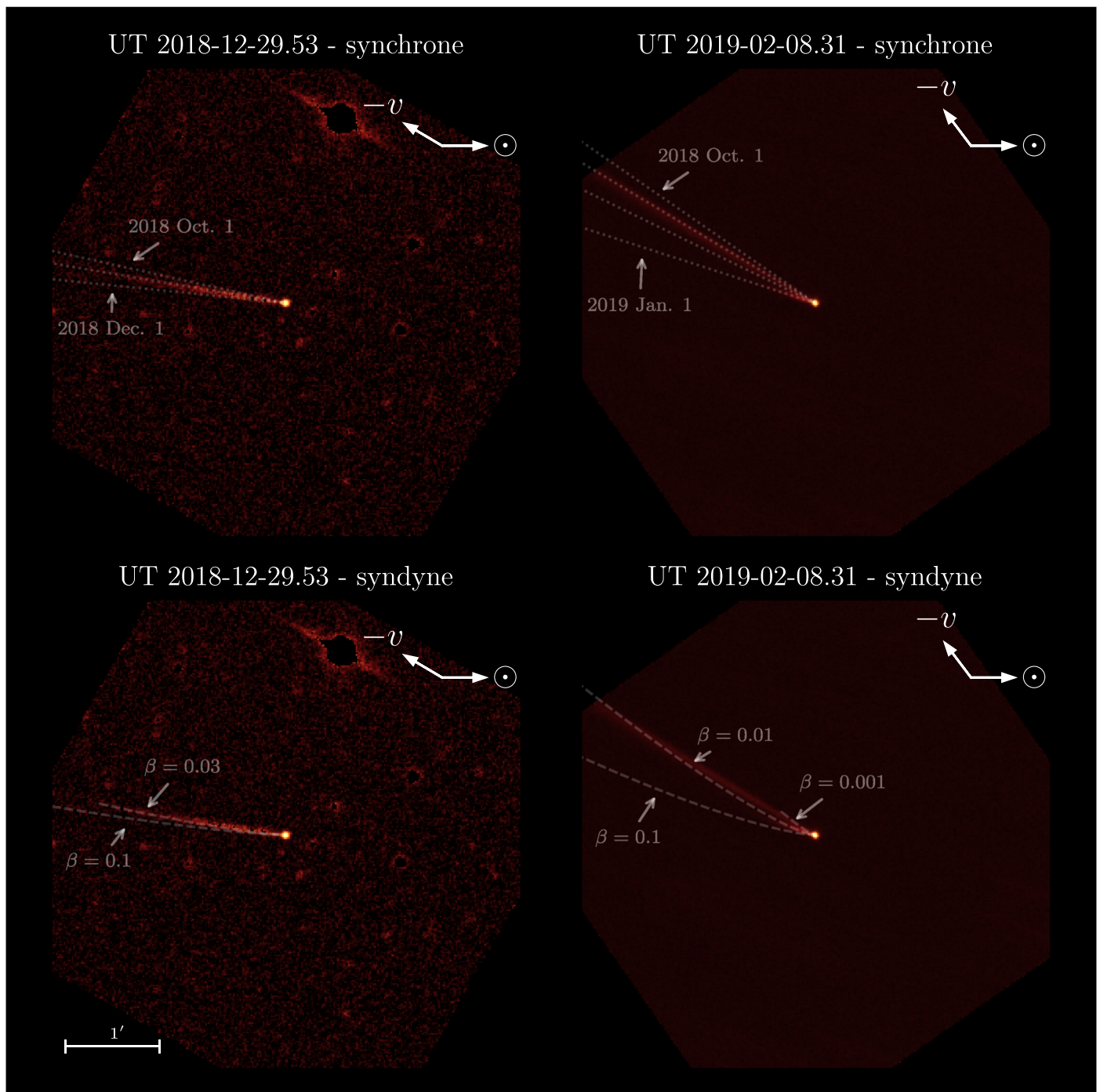


Figure 4. ZTF images from 2018 December 29 and 2019 February 8 overlaid with syndyne-synchrone chart. Synchrone lines are the position of particles released on 2018 October 1, November 1, December 1, and 2019 January 1 (for the 2019 February 8 image) in clockwise order. Syndyne lines are calculated for particles released after 2018 October 1. Notebook is available here https://github.com/Yeqzids/activation_of_6478_gault/blob/master/syndyne-synchrone.ipynb.

A merging binary system is expected to have a characteristic light curve with a large amplitude (Descamps 2008). The available ZTF data do not allow extraction of a rotational light curve; however, a crude inspection of Figure 2 does not show any noticeable scatter caused by large amplitude. This may be explained by the geometry between the orbital plane of the binary and the Earth, as well as the contamination of the ejecta. Future light-curve studies, to be conducted after the dust grains have moved away, should be able to prove or reject this theory.

6. Summary

We presented observations of newly identified active asteroid Gault obtained in the course of the ZTF survey. As of 2019 mid February, Gault exhibited two mass loss events: the first event started on 2018 October 18 ± 5 days, peaked around 2018 November 7, and subsided around 2018 mid December; the second event started on 2018 December 24 ± 1 days, peaked around 2019 January 4, and subsided around 2019 late-January. The two events released 2×10^7 kg

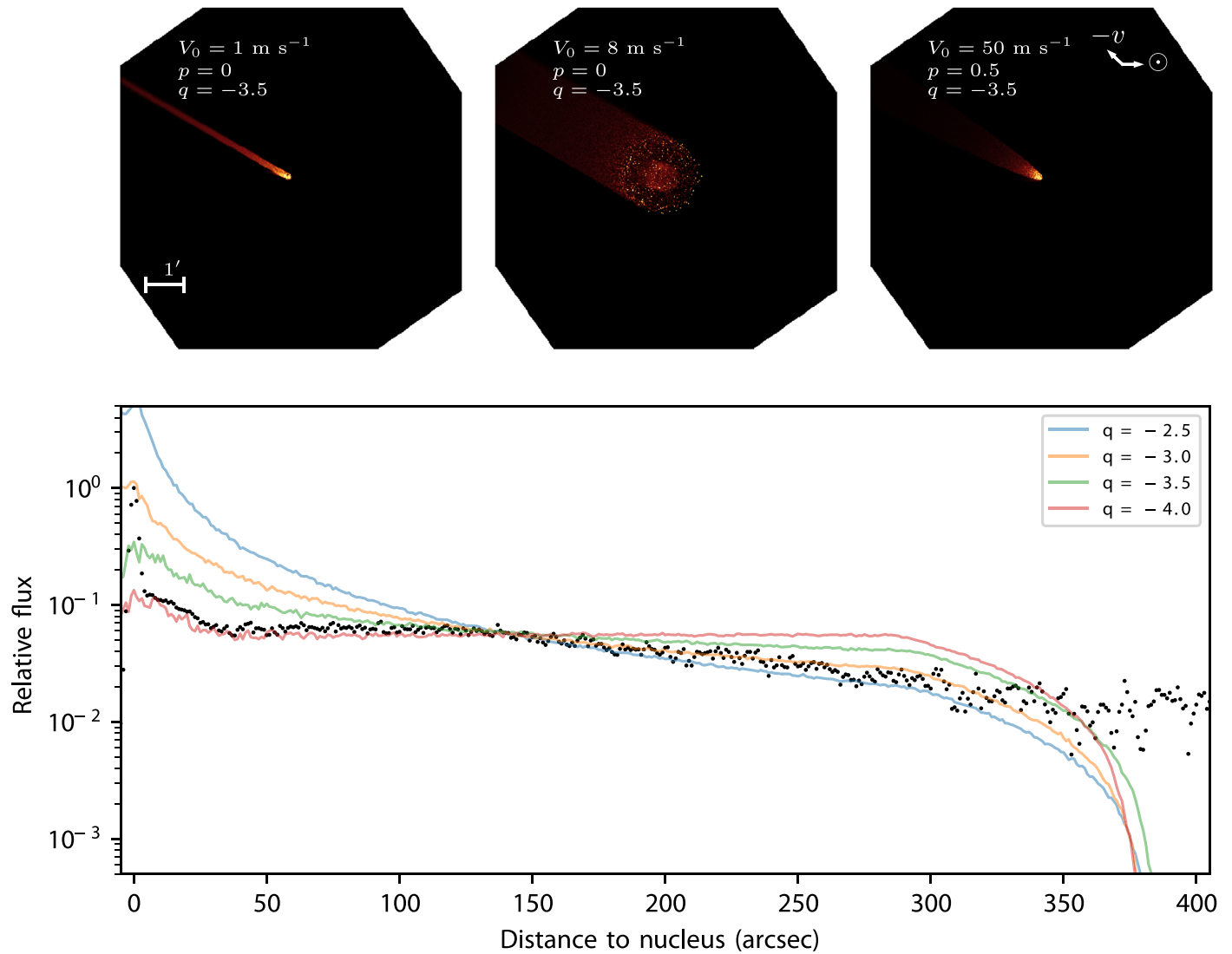


Figure 5. Dust tail model for the ZTF image taken on UT 2019 February 8.31. Upper panel: modeled images of three different sets of parameters. Lower panel: observed and modeled profile along the tail direction, normalized to the flux level at $140''$ (1.6×10^6 km at the asteroid) behind the nucleus. Notebook is available here https://github.com/Yeqzids/activation_of_6478_gault/blob/master/dust_model.ipynb.

and 1×10^6 kg of mass, respectively. Gault’s color did not change appreciably during the outbursts, with a pre-outburst color of $g_{\text{PS1}} - r_{\text{PS1}} = 0.50 \pm 0.04$ and $g_{\text{PS1}} - r_{\text{PS1}} = 0.46 \pm 0.04$ during the two outbursts.

We investigated the evolution of dust tail morphology using a dust dynamics model. We found that the ejecta was dominated by dust grains with sizes $\gtrsim 10 \mu\text{m}$, and followed different size distribution: particles at $10\text{--}20 \mu\text{m}$ follow a power law of -2.5 to -3.0 , while larger particles following a steeper slope of -4.0 . These particles were ejected at very low speeds of $\lesssim 1 \text{ m s}^{-1}$ regardless of particle sizes, consistent with non-sublimation-driven ejections observed in other active asteroids.

The derived properties were most consistent with activity driven by either rotational excitation, or merger of near-contact binaries. We showed that from a statistical perspective, a merger of near-contact binaries is more likely to be responsible for the activity of Gault, but additional observations are needed to prove or dispute this hypothesis.

We thank the referee for a prompt and helpful review, as well as Charles Bell and Man-To Hui for proofreading and comments. Q.-Z. Ye is supported by the GROWTH project funded by the National Science Foundation under grant No. 1545949. Bryce Bolin and Lynne Jones acknowledge support from the DIRAC Institute in the Department of Astronomy at the University of Washington. The DIRAC Institute is supported through generous gifts from the Charles and Lisa Simonyi Fund for Arts and Sciences, and the Washington Research Foundation. Funding for the Asteroid Institute program is provided by B612 Foundation, W.K. Bowes Jr. Foundation, P. Rawls Family Fund, and two anonymous donors in addition to general support from the B612 Founding Circle (https://b612foundation.org/member_group/founding-circle/).

This work is based on observations obtained with the Samuel Oschin Telescope 48 inch Telescope at the Palomar Observatory as part of the Zwicky Transient Facility project. Major funding has been provided by the U.S. National Science Foundation under

grant No. AST-1440341 and by the ZTF partner institutions: the California Institute of Technology, the Oskar Klein Centre, the Weizmann Institute of Science, the University of Maryland, the University of Washington, Deutsches Elektronen-Synchrotron, the University of Wisconsin-Milwaukee, and the TANGO Program of the University System of Taiwan.






This work made use of sbpy (<http://sbpy.org>), a community-driven Python package for small-body planetary astronomy supported by NASA PDART Grant 80NSSC18K0987.

Facility: PO:1.2 m.

Software: Astropy (Astropy Collaboration et al. 2018), Jupyter Notebooks (Kluyver et al. 2016), Matplotlib (Hunter 2007), MERCURY6 (Chambers & Migliorini 1997), sbpy (NASA-Planetary-Science/sbpy), ZChecker (mkelley/zchecker).

Note added. During the proofreading stage of this Letter, we learned of an independent paper by Kleyna et al. (2019) describing the original ATLAS detection of the event, as well as the *Hubble Space Telescope* and ground-based observations from a follow-up campaign. They independently reaches conclusions similar to those presented in this Letter.

ORCID iDs

Quanzhi Ye (叶泉志)  <https://orcid.org/0000-0002-4838-7676>
 Dennis Bodewits  <https://orcid.org/0000-0002-2668-7248>
 Lynne Jones  <https://orcid.org/0000-0001-5916-0031>
 Eric C. Bellm  <https://orcid.org/0000-0001-8018-5348>
 Dmitry A. Duv  <https://orcid.org/0000-0001-5060-8733>
 Shrinivas R. Kulkarni  <https://orcid.org/0000-0001-5390-8563>
 Thomas Kupfer  <https://orcid.org/0000-0002-6540-1484>
 Frank J. Masci  <https://orcid.org/0000-0002-8532-9395>
 Thomas A. Prince  <https://orcid.org/0000-0002-8850-3627>
 Maayane T. Soumagnac  <https://orcid.org/0000-0001-6753-1488>

References

Astropy Collaboration, Price-Whelan, A. M., Sipőcz, B. M., et al. 2018, *AJ*, 156, 123
 Bellm, E. C., Kulkarni, S. R., Graham, M. J., et al. 2019, *PASP*, 131, 018002
 Carry, B. 2012, *P&SS*, 73, 98
 Chambers, J. E., & Migliorini, F. 1997, *BAAS*, 29, 1024
 Chandler, C. O., Curtis, A. M., Mommert, M., Sheppard, S. S., & Trujillo, C. A. 2018, *PASP*, 130, 114502

Čuk, M. 2007, *ApJL*, 659, L57
 Čuk, M., & Burns, J. A. 2005, *Icar*, 176, 418
 Descamps, P. 2008, *P&SS*, 56, 1839
 Finson, M., & Probst, R. 1968, *ApJ*, 154, 327
 Fulle, M. 2004, in *Comets II*, ed. M. C. Festou, H. U. Keller, & H. A. Weaver (Tucson, AZ: Univ. Arizona Press), 565
 Fulle, M., Colangeli, L., Agarwal, J., et al. 2010, *A&A*, 522, A63
 Giorgini, J. D. 2015, *IAUGA*, 22, 2256293
 Gombosi, T. I. 1986, in *ESA Special Publication 250, ESLAB Symp. on the Exploration of Halley's Comet*, ed. E. J. Battrick, E. J. Rolfe, & R. Reinhard (Paris: ESA), 167
 Graham, M. J., Kulkarni, S. R., Bellm, E. C., et al. 2019, arXiv:1902.01945
 Hainaut, O. R., Boehnhardt, H., Snodgrass, C., et al. 2014, *A&A*, 563, A75
 Hale, A., Weiland, H., & Berry, R. 2019, *CBET*, 4597, 1
 Hsieh, H. H., Fitzsimmons, A., Joshi, Y., Christian, D., & Pollacco, D. L. 2010, *MNRAS*, 407, 1784
 Hui, M.-T., Jewitt, D., & Du, X. 2017, *AJ*, 153, 141
 Hunter, J. D. 2007, *CSE*, 9, 90
 Jehin, E. 2019, *CBET*, 4606, 1
 Jewitt, D., Hsieh, H., & Agarwal, J. 2015, in *Asteroids IV*, ed. P. Michel, F. E. DeMeo, & W. F. Bottke (Tucson, AZ: Univ. Arizona Press), 221
 Jurić, M., Ivezić, Ž., Lupton, R. H., et al. 2002, *AJ*, 124, 1776
 Kelley, M. S. P., Bodewits, D., Ye, Q., et al. 2019, in *ASP Conf. Ser. ADASS XXVIII*, ed. P. Teuben (San Francisco, CA: ASP) in press
 Klenya, J. T., Hainaut, O. R., Meech, K. J., et al. 2019, *ApJL*, in press
 Kluyver, T., Ragan-Kelley, B., Pérez, F., et al. 2016, *Jupyter Notebooks—A Publishing Format for Reproducible Computational Workflows* (Amsterdam: IOS Press),
 Lee, C.-H. 2019, *ATel*, 12468, 1
 Li, J.-Y., Helfenstein, P., Buratti, B., Takir, D., & Clark, B. E. 2015, in *Asteroids IV*, ed. P. Michel, F. E. DeMeo, & W. F. Bottke (Tucson, AZ: Univ. Arizona Press), 129
 Magnier, E. A., Schlafly, E., Finkbeiner, D., et al. 2013, *ApJS*, 205, 20
 Margot, J.-L., Pravec, P., Taylor, P., Carry, B., & Jacobson, S. 2015, in *Asteroids IV*, ed. P. Michel, F. E. DeMeo, & F. B. William (Tucson, AZ: Univ. Arizona Press), 355
 Marzari, F., Rossi, A., & Scheeres, D. J. 2011, *Icar*, 214, 622
 Masci, F. J., Laher, R. R., Rusholme, B., et al. 2019, *PASP*, 131, 018003
 Moreno, F., Licandro, J., & Cabrera-Lavers, A. 2012, *ApJL*, 761, L12
 Nesvorný, D. 2015, *PDSS*, 234
 Novaković, B., Tsirvoulis, G., Granvik, M., & Todović, A. 2017, *AJ*, 153, 266
 Pravec, P., Harris, A. W., Kušnirák, P., Galád, A., & Hornoch, K. 2012, *Icar*, 221, 365
 Price, M. C., Kearsley, A. T., Burchell, M. J., et al. 2010, *M&PS*, 45, 1409
 Rotundi, A., Sierks, H., Della Corte, V., et al. 2015, *Sci*, 347, aaa3905
 Schultz, P. H. 1999, *Icar*, 142, 1
 Smith, K., Denneau, L., Vincent, J.-B., & Weryk, R. 2019, *CBET*, 4594
 Taylor, P. A., & Margot, J.-L. 2014, *Icar*, 229, 418
 Willmer, C. N. A. 2018, *ApJS*, 236, 47
 Ye, Q., Kelley, M. S. P., Bodewits, D., et al. 2019, *ATel*, 12450
 Ye, Q., Wiegert, P. A., Brown, P. G., Campbell-Brown, M. D., & Weryk, R. J. 2014, *MNRAS*, 437, 3812
 Ye, Q.-Z., Brown, P. G., & Wiegert, P. A. 2016, *ApJL*, 818, L29